Research Article
Vol. 30, No. 24 / 21 Nov 2022 / Optics Express 42829
Optics EXPRESS

Chiral liquid crystal based holographic reflective lens for spectral detection

MIGLE STEBRYTE, INGE NYS, JEROEN BEECKMAN, AND KRISTIAAN NEYTS*

LCP Group, ELIS Department, Ghent University, Technologiepark-Zwijnaarde 126, 9052 Ghent, Belgium
*Kristiaan.Neyts@UGent.be

Abstract: Flat optics based on chiral liquid crystal (CLC) can be achieved using holographic polarization recording with the help of a photoalignment technique to vary the orientation of the optical axis in a thin CLC layer. A variety of reflective diffractive optical components with high efficiency and polarization selectivity can be realized employing this technique. In this work we discuss the use of CLC diffractive lenses in a spectrometer. The functionalities of two mirrors and a linear grating used in a traditional spectrometer are combined into a single holographic CLC component. Circularly polarized light entering through the slit can be reflected and projected onto a linear detector by the CLC component, with over 90% efficiency. This excellent optical functionality can be achieved with a micrometer thin CLC layer, offering the opportunity for device integration.

1. Introduction

A spectrometer is an essential instrument in many fields: basic research, bio-medicine, material characterization and product quality control [1]. Due to high demand in a wide range of applications there is a constant interest in making these instruments cheaper while maintaining high precision and speed.

The basic function of a spectrometer is to couple in light, split it into its spectral components and measure the intensity as a function of the wavelength. In a traditional Czerny-Turner spectrometer configuration light enters through a narrow slit and is collimated by a concave mirror into a parallel beam that is incident on a linear diffraction grating [2–4]. Since the diffraction angle is wavelength dependent, the light is separated into spectral components at different angles. A second concave mirror is transforming the parallel beams at different angles into different locations in the focal plane.

The diffraction grating is the essential component in the spectrometer design and there are two approaches to realize them: the ruled grating and the holographic grating. While the first is the most simple and the least expensive solution, the latter provides a more uniform spectral response and can be formed on a concave substrate and therefore provide both dispersive and focusing functionalities [5–10].

However, both types of gratings suffer from disadvantages. Ruled gratings, even though cheap to manufacture and relatively efficient (peak efficiency >80%), suffer from surface imperfections and errors in the groove period. As a result they produce much more stray light which is unacceptable for certain spectroscopic applications (such as Raman spectroscopy) [6]. Moreover, blazed gratings reach their peak efficiency for a particular design wavelength λ_B and the efficiency typically drops below 50% outside of the range $0.7\lambda_B$ to $1.8\lambda_B$ [7].

Holographic gratings are formed by interference between two beams which creates a sinusoidal refractive index variation in a photopolymer [8,9] or photopolymer with dispersed silver nanoparticles [10]. Therefore, the spectral response is uniform and very small periods can be achieved, down to a half wavelength of the light source used for interference illumination. However, the refractive index contrast achieved in these type of gratings is low (the order of 10^{-3})

#472821
Journal © 2022
https://doi.org/10.1364/OE.472821
Received 1 Sep 2022; revised 17 Oct 2022; accepted 24 Oct 2022; published 7 Nov 2022

Optics EXPRESS

and therefore they are rather inefficient (<35%) and are only used in cases when a small period and minimal ghosting effect is crucial.

In this work, we propose to employ flat optics based on chiral liquid crystal (CLC) to realize a new type of diffractive component to be used in a spectrometer. Reflective CLC gratings and lenses have recently drawn a lot of interest in the field of augmented and virtual reality display systems, because these components have a very high efficiency, large diffraction angles and polarization selectivity [11–16]. These components are fabricated by recording a polarization pattern on a photosensitive alignment layer using an interference setup [17]. A thin layer of liquid crystal is then deposited on top and the molecules align perpendicularly to the incident polarization direction during the photoalignmnet illumination [18,19]. This technique is similar to the case of holographic diffraction gratings mentioned before, even though in this case the interference illumination is done before the liquid crystal is put in contact with the alignment layer. Therefore, they are sharing the advantage of a uniform spectral profile and possibility to achieve sub-micrometer periods.

The material that CLC gratings are made of, self-organizes into a periodic helical structure and a photonic bandgap is formed. The bandgap depends on the helical pitch of the material and the refractive indices. Within a certain wavelength range, circularly polarized light with the same handedness as the material is reflected with close to 100% efficiency, which is much higher than for holographic diffraction gratings. As the refractive index contrast in the CLC is much higher (the order of 10^{-1}) than in case of the holographic gratings a highly efficient Bragg reflection can be achieved in CLC based diffraction gratings [20]. A CLC grating with a period close to 440 nm and an efficiency of >90% has been reported [21] and could be further improved using an antireflective coating. We have shown in our previous work that in case of a periodically rotating alignment at the surface CLC forms a structure with a tilted helical axis in the bulk of such component (Fig. 1). This gives rise to some interesting behaviour that is similar to a planar CLC with a light incident at an oblique angle [22].

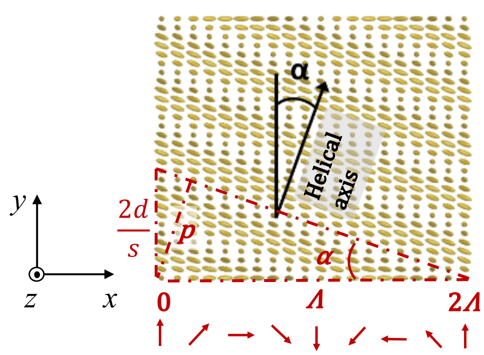

Fig. 1. Schematics of CLC grating with inclined helix, here α is the inclination angle of the helical axis, p is the helical pitch of the CLC, d is the thickness of the CLC layer and s the number of half-pitches, red arrows indicate the pattern of photo-alignment at the surfaces.

Using a similar technique, reflective CLC components can be made that combine grating and lens functionalities. The first reflective CLC-based lenses have been fabricated in 2016, but instead of an interference setup, an exposure system comprising a liquid crystal display projector and a rotatable waveplate was used to define the orientation patterns on the photoalignment layer [23]. A few years later another development was reported in which a CLC lens was fabricated using a transmissive Pancharatnam-Berry lens (PBL) as a master lens meaning that the parameters of such a lens were limited by the available PBLs. Nevertheless, lenses with f – number close to 0.3 were achieved [24]. An off-axis lens that can focus a collimated beam incoming at an angle was also recently realized based on an interference pattern [25,26] and holographic method using a template pattern [27]. In our work we rely on an interference setup in which two spherical waves interfere at an angle creating a pattern for a novel component that allows us to obtain an image of the entrance slit of a spectrometer and also spatially separate these images into its spectral components. After filling the device with a mixture that becomes a CLC below the transition temperature, a reflective lens is achieved with efficiency and polarization selectivity similar to those of a CLC grating.

In order to obtain an efficient spectrometer design, we combined two functionalities (that of a grating and of a lens) into a single holographic reflective component that both disperses and focuses the light. This effectively allows to combine the functionality of 3 optical components in one CLC layer: two concave mirrors and a diffraction grating. We provide a theoretical description of the operation principle, fabricate the components and characterize them, determine their optical properties and compare them with values obtained from the theoretical description. We propose this novel approach to a spectroscopic detection based on a simple flat CLC component that is easy to fabricate and due to our developed theoretical model allows the design freedom and does not require a specially designed template lenses.

2. Methods

2.1. Fabrication of the sample

The holographic reflective CLC lenses in this work are fabricated using the following procedure. First, ITO-coated glass substrates are cleaned by sonication in soap, acetone and isopropanol. Then, a photo-alignment material (Brilliant Yellow, Sigma Aldrich, 0.5 wt% in dimethylformamide) is spin-coated on top (3000 rpm, 30 s) and soft baked for 5 min at 90°C. A cell configuration is used in which two identical substrates are glued together with a UV curable glue (NOA68) containing spherical spacer balls 3 μm diameter), that define the thickness of the LC layer.

Such a cell is illuminated using the interference setup described in the section 2.1. The principle behind photoalignment is the cis-trans isomerization of azo-group-containing molecules during irradiation with linearly polarized light. After illumination, these molecules tend to align perpendicularly to the polarization direction of the illumination, and the director of the liquid crystal that is in contact with the photoalignment layer, follows this orientation. Therefore, by spatially varying the polarization orientation of the incoming light we can define a pattern in the liquid crystal director [18,19].

To obtain a CLC with the desired bandgap, the nematic liquid crystal E7 (Merck) was mixed with 5.7% of right-handed chiral dopant BDH 1305 (Merck), which resulted in a chiral pitch of $p \approx 320$ nm. Cells were filled with a mesogenic mixture above the nematic-isotropic phase transition point (57°C) with the help of capillary forces and then slowly cooled down to room temperature.

2.2. Photoalignment illumination setup

The photoalignment was achieved using the illumination setup depicted in Fig. 2. A blue laser (Coherent, $\lambda = 457$ nm) is used as a light source. The beam is expanded to a diameter of 20 mm and passes through a 50:50 beam-splitter. Two quarter-waveplates are used to transform linearly polarized light coming from the laser into circularly polarized light with opposite handedness. The mirrors are used to achieve a certain angle between the two beams and the lenses are placed in such a way that both beams are overlapping. While the spherical lens #1 is placed at a distance just below 2 x f_1 from the sample, the spherical lens #2 is placed at a distance much smaller than f_2 so that both beams have approximately the same size on the sample. The sample is illuminated for 6 minutes with a total intensity of about 100 mW (50 mW in each beam).

Optics EXPRESS

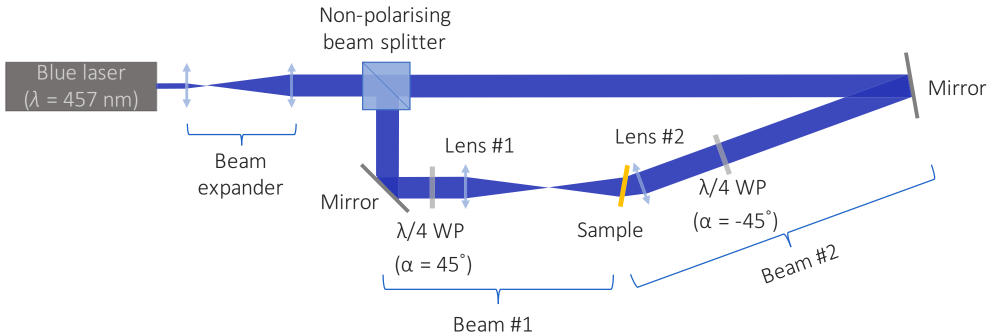

Fig. 2. Setup used to obtain a pattern for a holographic lens with use of interference of two spherical waves at an angle.

2.3. Theoretical background

A schematic that explains the reflective diffraction is depicted in Fig. 3(b). The light enters through a slit placed at a distance D_i at an angle θ_i with respect to the normal in the center of the component. It is reflected at an angle θ with respect to the surface normal and focused at a distance D, depending on the wavelength of the light. Since the component has diffractive properties, we define particular values θ_o and D_o for the wavelength λ_B that is used in the photo-alignment setup. In this case $\lambda_B = 457$ nm. The reflection angles and image distances (θ and D) for other wavelengths can be estimated from the following equations.

As can be seen in Fig. 3(a), in order to achieve the desired pattern, two blue laser beams with wavelength λ_B are incident from opposite sides of the sample at different angles and interfere at the surface coated by the photoalignment layer. To estimate the azimuthal angle of the resulting photoalignment orientation at the substrate surface, we determine the in-plane components of the optical electric field, which is the sum of the fields of the two interfering beams. Here the Gaussian beams used in the setup are approximated by two spherical waves:

$$\vec{E}_{tot} = (E_{i1}exp(-ik_BD_i) + E_{i2}exp(ik_BD_o))\vec{1}_x + i(-E_{i1}exp(-ik_BD_i) + E_{i2}exp(ik_BD_o))\vec{1}_y \quad (1)$$

Here E_{i1} and E_{i2} are the amplitudes of the two interfering beams, $\vec{1}_x$ and $\vec{1}_y$ are unit vectors along the x- and y- axis respectively and $k_B = 2\pi/\lambda_B$. When the amplitudes are equal, the field at z=0 is linearly polarized and we can determine the azimuthal angle φ_{tot} of the linear polarization:

$$\varphi_{tot} = -k_B\frac{D_o + D_i}{2} \quad (2)$$

According to the principle of photoalignment, the azimuthal angle of the liquid crystal director on the surface will be equal to $\varphi_{tot} + \pi/2$. For a given x_g coordinate on the grating sample the obtained angle can be rewritten as:

$$\varphi_{tot} = -\frac{\pi}{\lambda_B}\left(\sqrt{(x_o - x_g)^2 + z_o^2} + \sqrt{(x_i - x_g)^2 + z_i^2}\right) \quad (3)$$

with (x_o, z_o) and (x_i, z_i) the focal points of the two laser beams.

When light is reflected upon a CLC, it acquires a phase delay Γ_g, which is called the geometric or Pancharatnam-Berry phase [28]. This phase delay is two times larger than the azimuthal angle:

$$\Gamma_g = 2\varphi_{tot} \quad (4)$$

When light with wavelength λ is passing through the slit with coordinates (x_i, z_i) and subsequently reflected by the grating at coordinate $(x_g, 0)$, then the total phase delay at a coordinate (x, z) in

Optics EXPRESS

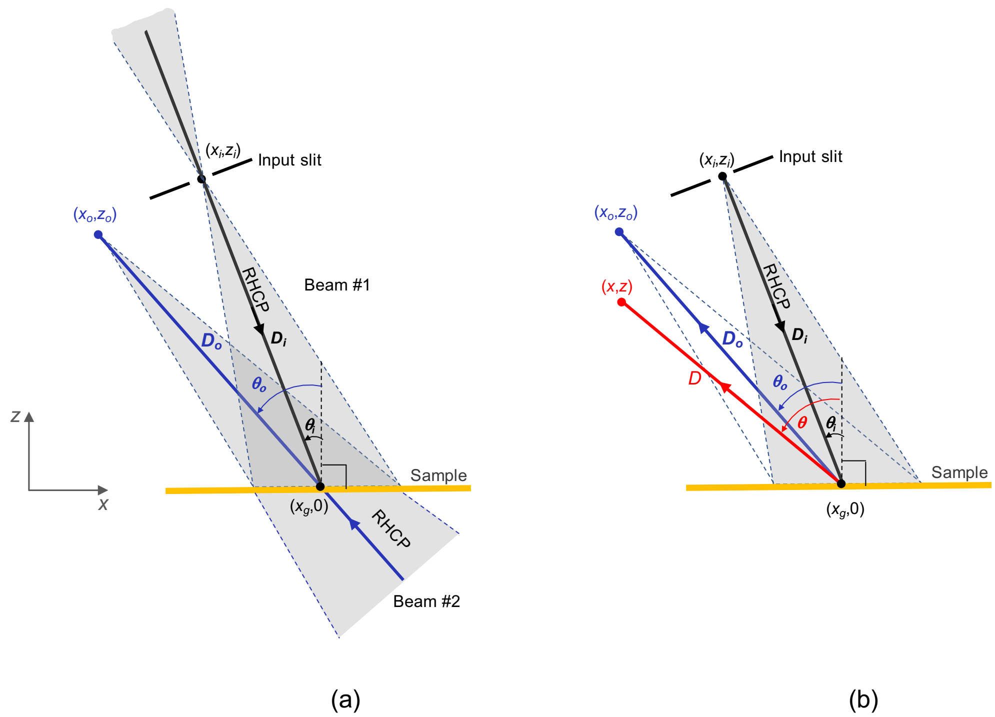

Fig. 3. Schematics for recording the interference pattern (a) and for the diffractive operation of the sample (b). (a) Interfering beams #1 and #2 are incident from opposite directions; (b) right-handed circularly polarized (RHCP) light is incident on the sample and the first order is diffracted at a certain angle. The blue arrow represents the path of the light with the same wavelength as used for the recording and the red arrow represents the path for a larger wavelength.

space is given by:

$$\Gamma_{tot} = \frac{2\pi}{\lambda_B}\left(\sqrt{(x-x_g)^2+z^2}+\sqrt{(x_i-x_g)^2+z_i^2}\right) - \frac{2\pi}{\lambda_B}\left(\sqrt{(x_o-x_g)^2+z_o^2}+\sqrt{(x_i-x_g)^2+z_i^2}\right) \tag{5}$$

To find the position (x, z) where the reflected light is focused, we require that the total phase delay Γ_{tot} should be independent of the coordinate x_g on the grating. Neglecting spherical aberrations, this reduces to:

$$\frac{d\Gamma_{tot}}{dx_g} = 0; \qquad \frac{d^2\Gamma_{tot}}{dx_g^2} = 0 \tag{6}$$

After calculating the derivatives we obtain the following equations:

$$\frac{2\pi}{\lambda}(\sin\theta_i + \sin\theta) = \frac{2\pi}{\lambda_B}(\sin\theta_i + \sin\theta_o) \tag{7}$$

$$\frac{2\pi}{\lambda}\left(\frac{\cos^2\theta_i}{D_i} + \frac{\cos^2\theta}{D}\right) = \frac{2\pi}{\lambda_B}\left(\frac{\cos^2\theta_i}{D_i} + \frac{\cos^2\theta_o}{D_o}\right) \tag{8}$$

This allows to subsequently calculate the diffraction angle θ and the distance D where the light is focused for a wavelength λ:

$$\sin\theta = \frac{\lambda}{\lambda_B}(\sin\theta_i + \sin\theta_o) - \sin\theta_i \tag{9}$$

Optics EXPRESS

$$D = \frac{1 - \sin^2\theta}{\frac{\lambda}{\lambda_B}\left(\frac{\cos^2\theta_i}{D_i} + \frac{\cos^2\theta_o}{D_o}\right) - \frac{\cos^2\theta_i}{D_i}} \tag{10}$$

Note that for $\lambda = \lambda_B$ these equations yield a focal point that is equal to the focal point of the second beam used for the illumination (x_o, z_o). For this wavelength, the imaging characteristics of the lens should be free of aberrations.

3. Result

A component with parameters listed in Table 1 has been fabricated and characterized. Figure 4 shows an image of the fabricated sample. The reflection in the green wavelength range is clearly visible. The diameter of the sample is 2 cm. Some scattering features are also present in the sample.

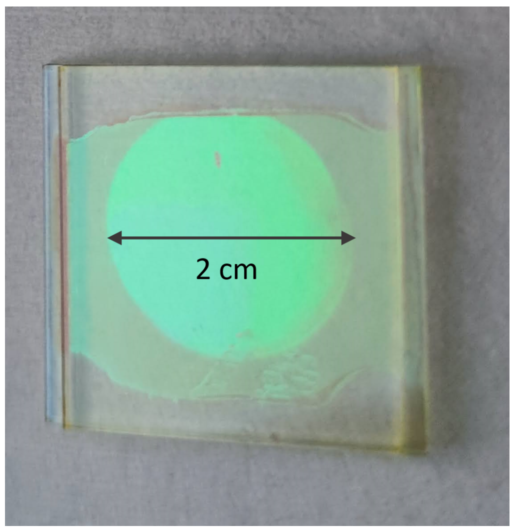

Fig. 4. Image of the CLC based holographic reflective lens sample.

Table 1. Photo-alignment setup parameters used to fabricate the sample.

	Recording@457 nm
D_i	17 cm
D_o	10 cm
θ_i	10°
θ_o	20°

After realizing the interference illumination step (Fig. 5), filling the cell, and cooling into the CLC phase, the sample was placed back in the illumination setup and the blue laser beam #1 of Fig. 3 (λ = 457 nm) was used to illuminate the component. As expected, the reflected beam was focused at the focal point of beam #2 that was used for the illumination.

The transmission spectra for different locations of the component are depicted in Fig. 6. Here, unpolarized white light was used. Since there is no anti-reflection coating on the glass substrates, part of the light is reflected from the air/glass interfaces and the component suffers from scattering

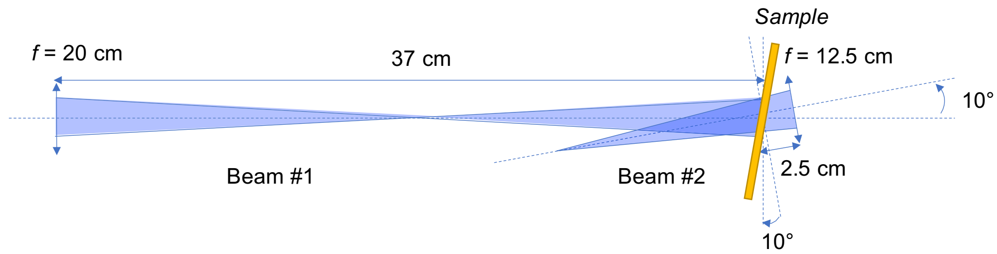

Fig. 5. Schematics of the illumination setup configuration used for the sample fabrication.

losses as well. Therefore the transmission does not reach 100% outside of the reflection band. A reflection band between 480 nm and 570 nm is observed. The spectra were measured at the centre and near the edges of the sample. Since the sample is designed to be used at 10° angle of incidence (in air), it was tilted over this angle when measuring the transmission spectra. We can observe side lobes in the transmission spectra, which oscillate faster in the shorter wavelength range, which is typical for CLC devices. It can also be observed that the reflection band is asymmetric with transmission lower at the short wavelength side. This asymmetry is due to the slanted helical structure in the bulk of the component, that is equivalent to a light incident on the planar CLC at an oblique angle [22].

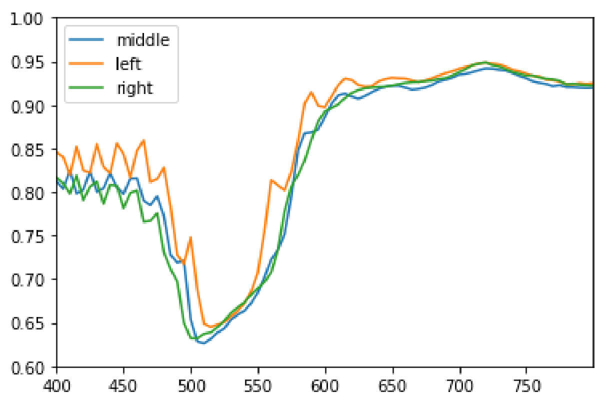

Fig. 6. Transmission spectra recorded near the left and right edges and in the middle of the sample. Unpolarized white light was used as a source and the sample was tilted over 10°.

Table 2 contains the theoretical and measured position of the focal point for different wavelengths, expressed as the distance D and the angle θ. The measurement was conducted using the same setup as the one used for the photoalignment illumination (Fig. 5), where the blue laser beam #1 was replaced by a white light source, with different color filters. The left side of the table represents the theoretical values for three wavelengths: 500 nm, 550 nm and 600 nm. Since the geometry of the incident beam is not changed, the values for θ_i and D_i remain constant. The values for θ and D are calculated using Eq. (9) and (10), respectively.

On the right side of Table 2 the measured values for the focal distance are presented for the same three wavelengths. The theoretical and measured values for the distance D agree very well, with the largest discrepancy being only 3 mm.

A slightly larger discrepancy is observed for the angle of the diffracted light θ. The increase of the angle with increasing wavelength is according to the theoretical model. The largest difference between the measured and theoretical values of 4° is observed at $\lambda = 550$ nm.

Optics EXPRESS

Table 2. Theoretical (left side) and experimentally measured (right side) positions of the focal point for three wavelengths: 500 nm, 550 nm and 600 nm.

	Theory			Measured		
	@500 nm	@550 nm	@600 nm	@500 nm	@550 nm	@600 nm
D_i	17 cm	17 cm	17 cm	17 cm	17 cm	17 cm
D	8.8 cm	7.5 cm	6.4 cm	8.5 cm	7.5 cm	6.5 cm
θ_i	10°	10°	10°	10°	10°	10°
θ	23°	26°	30°	21°	22°	27°

Finally, Fig. 7 demonstrates the imaging properties of the holographic reflective lens for different wavelengths. In the measurement setup, which is depicted in the middle of Fig. 7, we used a white LED as a light source. The light passes through a rectangular slit (2 mm x 8 mm), is reflected by the component and an image is formed on the screen. The sample is placed at the distance at which the light passing through the slit completely covers the lens, so we use the whole area. After the reflection, we can observe a focused image of the white light at a certain plane and with the use of color filters we can observe focused images for different wavelengths. From the images we can see that the three spots (for the three different color filters) are well separated in space on the image plane. The brightest image is obtained for λ = 550 nm which is in the center of the reflection band. As the wavelengths get further from the central wavelength the images become less bright.

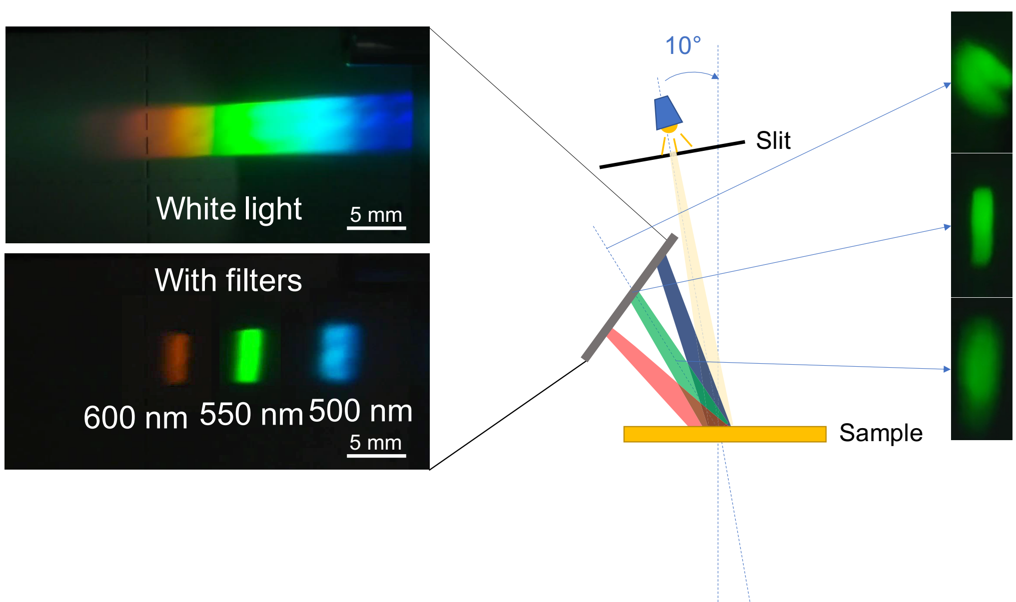

Fig. 7. Photographs of the images of the entrance slit obtained with the CLC based holographic reflective lens are shown on the left. The measurement setup is depicted in the middle. For the first photograph a white light source is used, and for the lower image, three photographs are combined for three different color filters (λ = 500 nm, λ = 550 nm and λ = 600 nm). On the right an image of the slit for the light of λ = 550 nm is shown at three different positions: behind the image plane, at the image plane and in front of image plane.

4. Discussion

The transmission spectra measured at several spots along the component show a slight shift in the reflection band (see Fig. 6), which is expected because of the varying periodicity in the surface alignment. For the yellow curve in Fig. 6, which was measured at the side with larger x-coordinate in Fig. 3(b), we see a narrowing of the bandgap which can be ascribed to a larger inclination angle of the helix and a smaller period of the photoalignment [22]. A smaller period in the alignment is expected because the light incident at this side has to be diffracted over a larger angle to reach the focal point.

The fact that the bandgap is rather narrow limits the detectable wavelengths range using a CLC based holographic reflective lens. One solution could be using liquid crystal with larger anisotropy, as the bandgap width is proportional to the birefringence: $n_o p < \lambda < n_e p$, where n_o and n_e are ordinary and extraordinary refractive indices, respectively, and p is the helical pitch. Another option is to stack several layers of CLC having different reflection bands to broaden the reflection wavelength range.

Table 2 shows a good agreement between experimental results and the theoretical prediction for the position of the focusing point for different wavelengths. It is quite straightforward to set the distances between different components. The prediction for the angle is not as accurate, which may be explained by the limited accuracy of the orientation angle in the recording setup, in particular for the orientation of lens #2.

The imaging properties of the component were evaluated for different wavelengths. As can be seen from Fig. 7 for the white light source, an image of the entrance slit is formed at an image plane for a wide range of the visible spectrum, even though the reflection band is only around 90 nm wide. This can be explained by the side lobes that are characteristic for the CLC reflection spectrum that covers a wide range of wavelengths. The reflection efficiency outside the reflection band is however rather low.

In the image where the color filters are used (Fig. 7, bottom left), the brightest image is for λ = 550 nm (center of the reflection band). It can also be observed that images for λ = 550 nm and λ = 600 nm are slightly deformed: going to a longer wavelength results in an image that is expanded laterally. This is because the screen can be perpendicular only to one of the beams and with the others it will have a small tilt angle which results in a deformation of the image. This effect could be minimized by using a more narrow slit. However, due to a weak light source and absorption of the color filters there was not enough light passing through a narrower slit to take a clear picture.

On the right side of Fig. 7 an image of the slit is depicted at λ = 550 nm at three different positions: behind the image plane, at the image plane and in front of an image plane. It is evident that a sharp image is obtained in one position and it gets out of focus as we move away from that position (image plane).

To form the images depicted in Fig. 7 the whole sample area was illuminated. A good quality of the slit images shows that the sample has a good optical quality across the whole area of π cm^2. However, as mentioned before some scattering features and defects are still present in the sample and further improvements are necessary. Having a large area component is important in spectrometer applications as it can capture more light. Even larger samples can be made using our method if needed and the high quality can be preserved across the sample area. However, it is important to keep in mind that the size of such components is limited by the optics size in the illumination setup, laser power and minimum period needed to achieve a desired diffraction angle and/or focusing power.

5. Conclusion

A holographic reflective lens was fabricated combining functionalities of a diffraction grating and a reflective lens. This novel design was achieved using an interference pattern that was based on our developed theoretical model and then confirmed by experimental characterization. Such a component can efficiently substitute spherical mirrors and a diffraction grating which are the essential components in a spectrometer and hence reduce the number of required optical components. Furthermore, such a CLC-based component can demonstrate a reflection efficiency of over 90% for circularly polarized light that is in the wavelength range of the CLC's photonic bandgap. The bandgap imposes a limitation on such a device, depending on the refractive indices and helical pitch. This limitation can be overcome by using a material with larger anisotropy, or by stacking several layers of CLC with different reflection bands.

A theoretical model was proposed and tested experimentally to calculate the coordinates of the focus for different wavelengths from the interference phase profile. Such model is necessary in order to be able to fabricate components for different spectrometer designs. The photoalignment technique used in this work provides a wide range of possible component designs and a theoretical background is necessary to be able to find the most suitable set of illumination setup parameters for a required application.

Funding. Fonds Wetenschappelijk Onderzoek (1S88222N, 3G0C2121).

Disclosures. The authors declare no conflicts of interest.

Data availability. No data were generated or analyzed in the presented research.

References

1. N. Savage, "Spectrometers," Nat. Photonics **3**(10), 601–602 (2009).
2. A. B. Shafer, L. R. Megill, and L. Droppleman, "Optimization of the czerny–turner spectrometer*," J. Opt. Soc. Am. **54**(7), 879–887 (1964).
3. D. R. Austin, T. Witting, and I. A. Walmsley, "Broadband astigmatism-free czerny-turner imaging spectrometer using spherical mirrors," Appl. Opt. **48**(19), 3846–3853 (2009).
4. K.-S. Lee, K. P. Thompson, and J. P. Rolland, "Broadband astigmatism-corrected czerny–turner spectrometer," Opt. Express **18**(22), 23378–23384 (2010).
5. L. E. Popov and E.G , *Diffraction Gratings and Applications* (1st ed.) (CRC Press, 1997).
6. J. Gao, P. Chen, L. Wu, B. Yu, and L. Qian, "A review on fabrication of blazed gratings," J. Phys. D: Appl. Phys. **54**(31), 313001 (2021).
7. E. G. Loewen, M. Nevière, and D. Maystre, "Grating efficiency theory as it applies to blazed and holographic gratings," Appl. Opt. **16**(10), 2711–2721 (1977).
8. N. George and J. W. Matthews, "Holographic diffraction gratings," Appl. Phys. Lett. **9**(5), 212–215 (1966).
9. W. gao Lu, R. Xiao, J. Liu, L. Wang, H. Zhong, and Y. Wang, "Large-area rainbow holographic diffraction gratings on a curved surface using transferred photopolymer films," Opt. Lett. **43**(4), 675–678 (2018).
10. A. K. Yetisen, H. Butt, F. da Cruz Vasconcellos, Y. Montelongo, C. A. B. Davidson, J. Blyth, L. Chan, J. B. Carmody, S. Vignolini, U. Steiner, J. J. Baumberg, T. D. Wilkinson, and C. R. Lowe, "Light-directed writing of chemically tunable narrow-band holographic sensors," Adv. Opt. Mater. **2**(3), 250–254 (2014).
11. J. Kobashi, H. Yoshida, and M. Ozaki, "Planar optics with patterned chiral liquid crystals," Nat. Photonics **10**(6), 389–392 (2016).
12. K. Yin, T. Zhan, J. Xiong, Z. He, and S.-T. Wu, "Polarization volume gratings for near-eye displays and novel photonic devices," Crystals **10**(7), 561 (2020).
13. Y.-H. Lee, K. Yin, and S.-T. Wu, "Reflective polarization volume gratings for high efficiency waveguide-coupling augmented reality displays," Opt. Express **25**(22), 27008–27014 (2017).
14. Y. Weng, Y. Zhang, J. Cui, A. Liu, Z. Shen, X. Li, and B. Wang, "Liquid-crystal-based polarization volume grating applied for full-color waveguide displays," Opt. Lett. **43**(23), 5773–5776 (2018).
15. I. Nys, M. Stebryte, Y. Y. Ussembayev, J. Beeckman, and K. Neyts, "Tilted chiral liquid crystal gratings for efficient large-angle diffraction," Adv. Opt. Mater. **7**(22), 1901364 (2019).
16. K. Yin, E.-L. Hsiang, J. Zou, Y. Li, Z. Yang, Q. Yang, P.-C. Lai, C.-L. Lin, and S.-T. Wu, "Advanced liquid crystal devices for augmented reality and virtual reality displays: principles and applications," Light: Sci. Appl. **11**(1), 161 (2022).
17. G. P. Crawford, J. N. Eakin, M. D. Radcliffe, A. Callan-Jones, and R. A. Pelcovits, "Liquid-crystal diffraction gratings using polarization holography alignment techniques," J. Appl. Phys. **98**(12), 123102 (2005).
18. O. Yaroshchuk and Y. Reznikov, "Photoalignment of liquid crystals: basics and current trends," J. Mater. Chem. **22**(2), 286–300 (2012).

19. V. G. Chigrinov, "Photoaligning and photopatterning - a new challenge in liquid crystal photonics," Crystals **3**(1), 149–162 (2013).
20. M. Mitov, "Cholesteric liquid crystals with a broad light reflection band," Adv. Mater. **24**(47), 6260–6276 (2012).
21. Y.-H. Lee, Z. He, and S.-T. Wu, "Optical properties of reflective liquid crystal polarization volume gratings," J. Opt. Soc. Am. B **36**(5), D9–D12 (2019).
22. M. Stebryte, I. Nys, Y. Y. Ussembayev, J. Beeckman, and K. Neyts, "Large angle forward diffraction by chiral liquid crystal gratings with inclined helical axis," Crystals **10**(9), 807 (2020).
23. K. M. Lee, M. Rumi, M. S. Mills, V. Reshetnyak, D. R. Evans, T. J. Bunning, and M. E. McConney, "A different perspective on cholesteric liquid crystals reveals unique color and polarization changes," ACS Appl. Mater. Interfaces **12**(33), 37400–37408 (2020).
24. Y. Li, T. Zhan, and S.-T. Wu, "Flat cholesteric liquid crystal polymeric lens with low f-number," Opt. Express **28**(4), 5875–5882 (2020).
25. J. Xiong, G. Tan, T. Zhan, and S.-T. Wu, "Breaking the field-of-view limit in augmented reality with a scanning waveguide display," OSA Continuum **3**(10), 2730–2740 (2020).
26. K. Yin, Z. He, and S.-T. Wu, "Reflective polarization volume lens with small f-number and large diffraction angle," Adv. Opt. Mater. **8**(11), 2000170 (2020).
27. J. Xiong, Q. Yang, Y. Li, and S.-T. Wu, "Holo-imprinting polarization optics with a reflective liquid crystal hologram template," Light: Sci. Appl. **11**(1), 54 (2022).
28. M. Berry, "The adiabatic phase and pancharatnam's phase for polarized light," J. Mod. Opt. **34**(11), 1401–1407 (1987).